Research Article

Khalid Maniah*

Antifungal, antioxidant, and photocatalytic activities of greenly synthesized iron oxide nanoparticles

https://doi.org/10.1515/chem-2024-0031
received January 23, 2024; accepted April 16, 2024

Abstract: The build-up of synthetic dyes in the environment and aquatic ecology is a significant environmental issue due to their inability to break down naturally. The overuse of chemical fungicides also poses a threat to the environment due to their accumulation and fostering of fungal resistance. Hence, the study was conducted to detect the antifungal properties and photocatalytic activity of greenly synthesized iron oxide nanoparticles (IONPs) prepared using the *Hibiscus sabdariffa* flower extract. The biogenic IONPs showed the highest photocatalytic activity against rhodamine B dye at a concentration of 4.0 mg/ml. The biogenic IONPs also demonstrated effective antifungal properties against *Penicillium digitatum* and *Aspergillus niger* strains, with relative inhibition percentages of mycelial growth being higher than those with the metalaxyl + mancozeb fungicide at 800 ppm concentration. The efficient photocatalytic activity of the biogenic IONPs against rhodamine B dye and their effective antifungal properties suggest their potential use as safe substitutes for commercial fungicides.

Keywords: *Hibiscus sabdariffa*, iron oxide nanoparticles, characterization, rhodamine B, antifungal, antioxidant

1 Introduction

Water is an essential component necessary for the sustenance of life on the earth. Similar to all living things, humans are completely reliant on water for their daily life [1]. The depletion of water supplies is progressively occurring as a result of overuse [2]. Increasing water contamination presents a significant peril to the well-being of all organisms and the earth [3]. The primary origins of illnesses caused by water contamination are the presence of dangerous and poisonous chemicals or biological waste, which originate from manufacturing companies, residential areas, and several other sources [4]. Rhodamine B dyes are used in a variety of industries, including the textile, chemical, pharmaceutical, paper, and cosmetic sectors [5]. As a result, a significant amount of toxic substances infiltrate water sources and pollute natural water reservoirs. The intake of these dyes can lead to the development of cancer due to the presence of aromatic amines in their composition [6]. This is the rationale behind the implementation of environmental regulations, which mandate businesses to eliminate these deleterious substances from contaminated industrial fluids prior to their discharge into the natural surroundings [7]. Dyes are widely used in many sectors, such as plastic, leather, textile, cosmetics, food, paper, and pharmaceutical, to impart color to the end goods [8]. The presence of dyes in industrial wastewater, even in minuscule amounts, may have a substantial influence on the environment and pose dangers to aquatic creatures and human health [9]. Various common techniques exist for eliminating colors from industrial wastewater (effluents). The methods used for treatment include biological treatment, coagulation/flocculation, ozonation, electrodialysis, membrane separation, adsorption on a solid phase, electrochemical oxidation, sorption-floatation, ultrafiltration, and Fenton/photo-Fenton oxidation [10]. Nevertheless, these procedures are subject to many restrictions, such as the extended duration required for biological treatment processes and the emission of unpleasant odors [11]. Moreover, incineration may generate hazardous volatile gases [12]. Ozonation has a brief half-life of 20 min, and the stability of ozone is significantly influenced by factors such as pH, salts, and temperature [13]. Additionally, ozonation is costly and inefficient, and leads to the production of substantial amounts of sludge and by-products [14]. Recently, it has been revealed that metal/metal oxide nanoparticles (NPs) are efficient photocatalysts for the degradation of

*** Corresponding author: Khalid Maniah,** Department of Biology, King Khalid Military Academy, P.O. Box 22140, Riyadh, Saudi Arabia, e-mail: Khalede_sa@hotmail.com

dyes [15]. This process occurs at ambient temperature and is activated by visible light irradiation [16]. Photocatalysis is a process in which organic molecules are either reduced or oxidized by redox processes triggered by light. The activation of these processes occurs when electron–hole pairs are produced on the surface of semiconductors (metal oxide) following exposure to light that exceeds the bandgap energy [17]. Photocatalytic technology has garnered significant attention in the realm of water pollution prevention [18]. The photocatalyst operates on the idea of using solar energy to facilitate the oxidation process of various pollutants present in water [19]. This approach facilitates the oxidative removal of many pollutants, including organic chemical compounds, microbes, and micropollutants such as antibiotics and dyes [20]. Nanomaterials, which have dimensions ranging from 1 to 100 nm, exhibit unique structural and physicochemical characteristics in comparison to their bulk counterparts due to the surface-to-volume ratio [21]. The latest progress in the field of nanotechnology has resulted in an increased scope for the production of NPs by various chemical and physical techniques [22]. Nevertheless, the use of these technologies has been found to have adverse effects on the environment and living species since unreacted chemicals are released into the surrounding environment [23]. Hence, it is imperative to produce NPs utilizing environmentally friendly methods. Biogenically synthesized NPs may be effectively utilized in several fields such as electronics, material science, medicinal applications, and environmental remediation [24]. The features of metal oxide NPs have generated significant attention in the field of catalysts due to their distinct and complex characteristics [25]. NPs are of significant importance in the removal of many contaminants. Metal oxide NPs have become more popular for the purpose of remediating environmental pollutants present in air, water, and soil [26]. Current research has shown that metal oxide NPs exhibit a high level of efficacy in the process of color dye degradation [27]. In recent times, there has been a significant amount of attention directed at iron oxide nanoparticles (IONPs) owing to their distinctive characteristics, including superparamagnetism, increased surface area, and convenient separation techniques [28]. In their study, Muthukumar and Matheswaran documented the use of *Amaranthus spinosus* leaf extract for the eco-friendly production of IONPs with spherical morphology and a rhombohedral crystal structure. The average diameter of these NPs was measured to be 91 nm, recording relative color removal percentages of 75 ± 2 and 69 ± 2% for methyl orange and methylene blue, respectively [29]. Alagiri and Hamid conducted a study whereby they documented the process of synthesizing Fe_2O_3 NPs using a green approach, utilizing *Curcuma* and tea leaves as the primary sources, producing IONPs of average crystalline diameters of 4 and 5 nm, respectively. These IONPs showed photocatalytic degradation of methyl orange dye within 120 min under visible light irradiation [30]. Additionally, a prior investigation showcased the creation of a nanocomposite consisting of iron oxide and activated carbon (Fe_3O_4/AC) for the purpose of eliminating Congo Red (CR) dye. The nanocomposite exhibited a biosorption capacity of 122.22 mg/g for the dye at pH 5–6, using a dosage of 0.04 g of Fe_3O_4/AC at a dye concentration of 40 mg/l [31]. However, several research studies have documented other methods for removing organic colors from aquatic environments. Specifically, the use of fungal and bacterial laccase has mostly been focused on decolorization applications. Furthermore, the recyclability and increased operational stability of the laccase may be attained by the entrapment or immobilization of the enzyme [32]. A previous study revealed the development of a new biopolymer adsorbent with strong adsorptive ability against Direct blue (DB) and CR dyes, with maximum adsorptive capacities of 519.53 and 534.25 mg/g for CR and DB removal, respectively [33]. Moreover, oxidant-modified biochar was used to remove basic fuchsin from water systems by adsorption. The maximum removal efficiency, reaching 98.28%, is achieved at a pH of 6.0 using 0.05 g of adsorbent at an initial pollutant concentration of 10 mg/l [34]. The disposal of organic and inorganic waste generated by many industrial sectors, including textiles, cosmetics, leather, paper, medicine, paint, and food production facilities, significantly contributes to environmental contamination and disrupts ecological balance. Rhodamine B, a cationic dye, exhibits toxicity toward living organisms and possesses carcinogenic and mutagenic properties. The presence of contaminants in drinking water has been associated with the development of sarcomas, as well as neurological and reproductive effects [35]. Hence, it is imperative to treat wastewater containing these colors in order to save the ecosystem and living organisms. Additionally, the excessive utilization of chemical fungicides presents a significant environmental hazard. Therefore, there is an urgent need to find safe and biogenic alternatives to chemical fungicides [36]. *Hibiscus sabdariffa* L. (roselle) is a well-recognized blooming plant that has over 300 species and is prevalent in tropical and subtropical regions around the globe [37]. Multiple studies have shown that the calyces of roselle contain a significant amount of polyphenols and flavonoids, which enhance the nutritional value of roselle due to their association with antioxidant activity [38]. The plant contains a high amount of phenolic compounds, specifically anthocyanins like sambubioside, delphinidin-3-glucoside, and cyanidine-3-sambubioside [39]. It also contains flavonoids such as gossypetine and hibiscetin, along with their respective glycosides. Other compounds present include eugenol, protocatechuic acid, and sterols like ergoesterol and β-

sitoesterol [40]. The extract's significant phenolic content highlights its potential as a stabilizing and reducing agent for metal ions [41]. Therefore, the present study aimed to synthesize IONPs environmentally using an aqueous extract derived from *Hibiscus sabdariffa* flowers. The NPs were subsequently characterized using various physicochemical techniques, and their photocatalytic efficacy in the degradation of rhodamine B dye was examined under both dark and sunlight conditions. Furthermore, the antifungal efficacy of the biogenic IONPs was assessed against two strains of rot fungus, namely *Penicillium digitatum* and *Aspergillus niger*, and compared to the commercially used fungicide known as metalaxyl + mancozeb.

2 Materials and methods

2.1 Preparation of the *H. sabdariffa* flower extract

Hibiscus sabdariffa desiccated flowers were purchased at a local market in Riyadh, Saudi Arabia. The herbarium confirmed the identification of the plant specimens. Following an initial washing with tap water, the dried flowers of *H. sabdariffa* were purified three times with distilled water. They were then placed in the shade to dry completely. Using a mechanical blender, the flowers were pulverized into a homogenous and finely powdered powder. A 500 ml flask was used to which 50 g of plant powder and 200 ml of distilled water were added. A hot plate was used to heat the flask to 60°C for 30 min. The flask was then subjected to continuous agitation at 25°C for 24 h, aided by a magnetic stirrer. Next, the mixture was purified using Whatman filter paper (1) in order to get a refined filtrate and remove any remaining impurities. Afterward, the aqueous extract was sterilized by filtering utilizing a 0.45 µm Millipore membrane filter. Finally, the sterilized extract was refrigerated at 4°C to reserve it for subsequent experimentations [42,43].

2.2 Ecofriendly formulation of IONPs

Ferric nitrate ($Fe(NO_3)_3{\cdot}9H_2O$, 0.01 M) was mixed with the water extract of *H. sabdariffa* flowers in a 1:1 ratio. The emergence of a black color signifies the prospective formation of IONPs. The reduced mixture was subjected to centrifugation at a speed of 10,000 rpm for a duration of 10 min. Following the centrifugation process, the supernatant was then separated and subsequently discarded. To completely remove any residues, the remaining IONP pellets were washed three times with distilled water [36,44].

2.3 Characterization of biogenic IONPs

Physicochemical techniques were utilized to characterize NPs, comprising the application of UV-Vis spectroscopy to determine the optical properties of NPs. The analysis of the morphology and size distribution of NPs was performed utilizing transmission electron microscopy (TEM) analysis; however, the assessment of the elemental map of NPs was conducted utilizing energy-dispersive X-ray (EDX) analysis. Moreover, Fourier transform infrared spectroscopy (FTIR) analysis identified the primary functional groups present in NPs. The bioprepared NPs were investigated by X-ray powder diffraction (XRD) to verify their crystalline nature. The Zeta sizer equipment (Malvern Instruments Ltd., Worcestershire, UK) was utilized to assess the surface charge and average diameter of NPs in colloidal solutions.

2.4 Photocatalytic degradation of rhodamine B dye using IONPs

The rhodamine B dye decolorization was evaluated by investigating various NP concentrations (0.5, 1.0, 2.0, and 4.0 mg ml^{-1}) and varied reaction periods (30.0, 60.0, 90.0, 120.0, 150.0, 180.0, and 210.0 min). The decolorization degree in relation to sunlight irradiation was evaluated under two conditions: an average solar irradiation of 1,000 W/m^2 at 38 ± 2°C, and in dark conditions. To achieve the condition of absorption/desorption equilibrium, a solution with 10 mg l^{-1} rhodamine B dye with NPs was exposed to constant spinning for a period of 30 min before initiating the photocatalytic experiment. The assessment of decolorization efficacy was conducted utilizing the following procedure: 1.0 ml was collected from each treatment and thereafter centrifuged at a speed of 10,000 rpm for a duration of 30 min. Subsequently, the obtained samples were analyzed to determine their optical density at the wavelength that corresponds to λ_{max} of the rhodamine B dye (554 nm). The analysis was conducted using a spectrophotometer (model 721, produced by M-ETCAL). The degradation percentage of the rhodamine B dye was determined by the following equation:

$$\text{The removal percentage of Dye}(D(\%)) = [\text{Dye(i)} - \text{Dye(f)}/\text{Dye(i)}] \times 100,$$

where dye (i) is the initial absorbance, and dye (f) is the final absorbance obtained at different time periods.

2.5 Total organic carbon (TOC) and chemical oxygen demand (COD) analysis

In order to affirm the full breakdown of rhodamine B dye, it is necessary to assess the photodegradation of a sample by measuring the decrease in TOC and COD. The degradation rate is determined by measuring COD and TOC using a HANNA HI93754A-25GB COD analyzer. The sample (2 ml) was put into many tubes and then placed in the reactor for 2 h at a temperature of 150°C. The COD removal percentage was determined using the following formula:

$$\text{COD removal (\%)} = ((\text{COD}_0 - \text{COD})/\text{COD}_0) \times 100.$$

The concentration of TOC was determined using a Hach DR-2800 TOC analyzer. About 10 ml samples were taken and the TOC removal percentage was determined using the following equation:

$$\text{TOC removal (\%)} = ((\text{TOC}_0 - \text{TOC})/\text{TOC}_0) \times 100.$$

The HPLC procedure was conducted using an XDB-C18 column with dimensions of 5 µm and 4.6 mm × 150 mm, maintained at a temperature of 30°C. The HPLC separation was conducted by using methanol as the eluent solvent, with a gradual increase in the methanol concentration from 60 to 90% over a duration of 15 min. The separation was performed at a 1 ml/min flow rate. Compounds were identified utilizing a UV detector set to a wavelength of 553 nm.

2.6 Antimicrobial activity of biogenic IONPs and standard fungicide against the tested fungal pathogens

Two pathogenic strains, namely *P. digitatum* ON201443 and *A. niger* ON197883, were investigated for their susceptibility to the NPs and chemical fungicide. The food poisoning assay was utilized to evaluate the antimicrobial proficiency of NPs and compared it with the commercially available metalaxyl + mancozeb fungicide, against the tested pathogenic microbes. Different dilutions of biogenic IONPs and fungicide (50, 100, 200, 400, and 800 ppm) were added to the sterilized PDA medium. Following this, a 6 mm disc of each fungal pathogen was used to inoculate the plates, which were then incubated at 25 ± 2°C for 7 days. Conversely, control plates were used, where just a 6 mm disc of microbial growth was introduced. The pathogenic fungus strain's growth diameter was evaluated using a Vernier caliper.

$$\text{The fungal inhibition (\%)} = (A - B)/A \times 100,$$

where A is the fungal growth diameter measured in control, and B is the fungal growth diameter recorded in the treatments.

The broth dilution technique was used to determine the minimum inhibitory concentration (MIC) values for the biogenic IONPs that exhibit antifungal activity against the tested pathogens. The MIC is the lowest concentration of the test sample at which the fungus exhibits no growth. The MIC values were determined by testing several concentrations (ranging from 1.000 to 0.002 mg/ml) of IONPs against the tested pathogens. The concentrations used were 1.000, 0.500, 0.250, 0.125, 0.063, 0.032, 0.016, 0.008, 0.004, and 0.002 mg/ml. A solution with an initial concentration of 1 mg/ml was prepared using the precipitated NPs. This solution was then diluted in a two-fold serial dilution. Then, 1 ml of each NP concentration was introduced to the test tubes, each containing 1 ml of the SDA broth. The tubes were thereafter injected with a standardized volume of fungal spore suspension containing 3×10^3 CFU/ml. The spore suspension was prepared from a fungal culture that had been grown for 5 days. The tubes were then incubated at 25°C for 48 h [45].

2.7 Antioxidant assay

The DPPH (2,2-diphenyl-1-picryl-hydrazyl) test is a commonly used technique for assessing antioxidant activity. Undoubtedly, DPPH is distinguished by its capacity to generate enduring free radicals. The stability of the molecule is a result of the dispersion of unbound electrons within it. The presence of these DPPH radicals causes the solution to appear dark violet since it absorbs radiation at around 517 nm. Different dilutions (50, 100, 150, 200, 250, and 500 mg/ml) of NPs were produced by disbanding them in methanol; 1 mM solution of DPPH was prepared by disbanding it in 100 ml methanol. The biogenic IONPs at different concentrations were combined with a 2 ml aliquot of DPPH solution. The solution was incubated at 25°C for 30 min in the dark. Ascorbic acid served as the positive control, whereas an equivalent amount of DPPH and methanol acted as the blank.

The percentage of DPPH scavenging may be calculated using the following formula:

$$\% \text{ DPPH scavenging} = [(A - B)/A] \times 100,$$

where A represents the absorbance of the control, and B represents the absorbance of the sample.

2.8 Statistical analysis

The research data were statistically investigated using GraphPad Prism version 8.0 (GraphPad Software, Inc., La Jolla, CA, USA) by a Tukey test or one-way ANOVA with a significance level of 0.05. The data are presented as the average of triplicates ± standard error.

3 Results and discussion

3.1 Ecofriendly formulation of NPs

The phytoconstituents present in the extract of *H. sabdariffa* flowers serve as both capping and reducing agents for the yellowish solution of ferric nitrate. This leads to the development of a reddish-black solution containing biogenic IONPs, as shown in Figure 1.

3.2 UV analysis of the biogenic IONPs

The extract of *H. sabdariffa* flowers and biogenic IONPs were examined using UV spectroscopy to evaluate the surface plasmon resonance (SPR) of the IONPs synthesized by plant-based methods. The analysis of the plant extract and the biogenic IONPs demonstrated the presence of two separate peaks at 240 and 257 nm, respectively. These peaks are likely attributed to the capping biomolecules present in the plant extract. Additionally, the UV spectrum of NPs displayed a broad peak at 476 nm, which could be accredited to the SPR of NPs (Figure 2). The outcomes of our research aligned with those of an earlier investigation, which showcased the SPR of zero-valent IONPs derived from *Isaria fumosorosea* at a wavelength of 470 nm [46]. Another research has shown the emergence of a wide absorption band within the visible spectrum, ranging from 470 to 550 nm. This occurrence signifies the SPR of IONPs [47]. The Tauc plot method was employed to detect the band gap energy of NPs to be 3.56 eV (Figure 3). A previous work showcased the environmentally friendly synthesis of IONPs with the ability to potentially degrade methylene blue dye by photocatalysis. These NPs were produced using the henna leaf extract and exhibited a band gap energy of

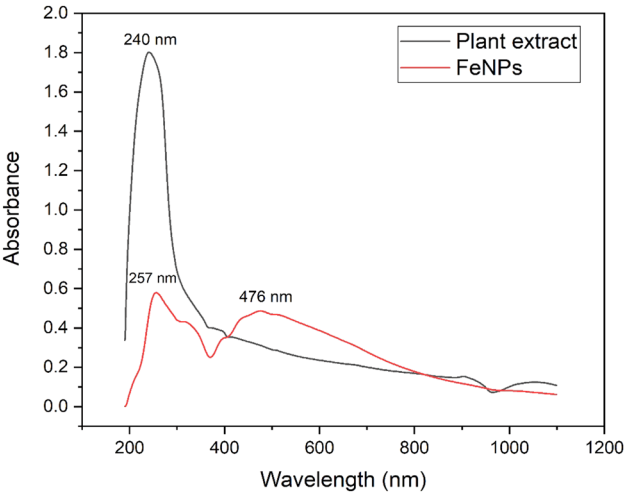

Figure 2: UV spectrum of the biogenic IONPs.

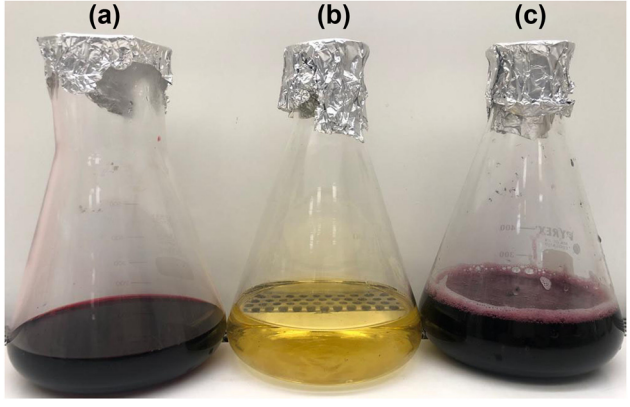

Figure 1: Green synthesis of biogenic IONPs (a: *H. sabdariffa* extract; b: ferric nitrate solution; c: biogenic IONPs).

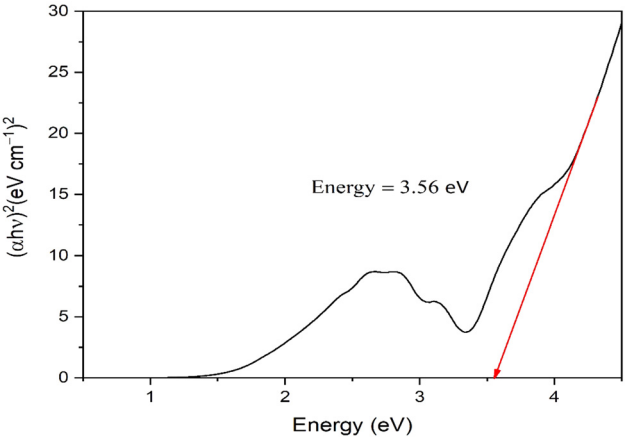

Figure 3: Band gap energy of the biogenic IONPs.

3.3 eV [48]. Furthermore, another research examined the band gap energy of IONPs by using *Avicennia marina* dry fruit. The results indicated a relative band gap energy of 3.16 eV [49].

3.3 TEM investigation of NPs

The biosynthesized IONPs were subjected to analysis via TEM to determine their shape, size, and particle size distributions. TEM images revealed the presence of extracellular matrix, which may be attributed to the phytoconstituents present in the plant extract used for the biosynthesis of IONPs. This finding was further confirmed using FTIR investigation, which showed the presence of several functional groups such as alcohols, alkanes, conjugated aldehydes, alkenes, phenols, amines, and primary alcohols capped over the surface of the biogenic IONPs. The NPs were spherical (Figure 4) with a diameter of 41.52 ± 14.8 nm (Figure 5).

3.4 EDX analysis of the biogenic IONPs

The EDX investigation of the bioinspired IONPs revealed the detection of Fe peaks at 0.8, 6.4, and 7.0 keV, which corresponded to the signals of Fe La, Fe Ka, and Fe Kb, respectively (Figure 6). Elemental mapping of NPs displayed the presence of carbon, oxygen, and iron with relative mass percentages of 77.44, 5.02 and 17.54%, respectively. In this

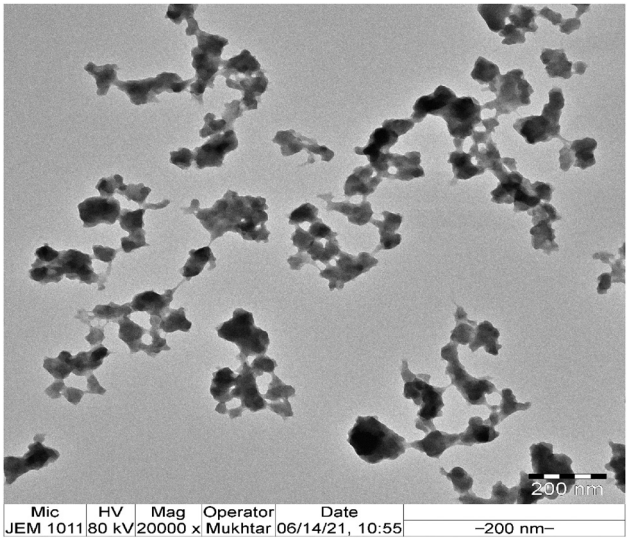

Figure 4: TEM images of the biogenic IONPs.

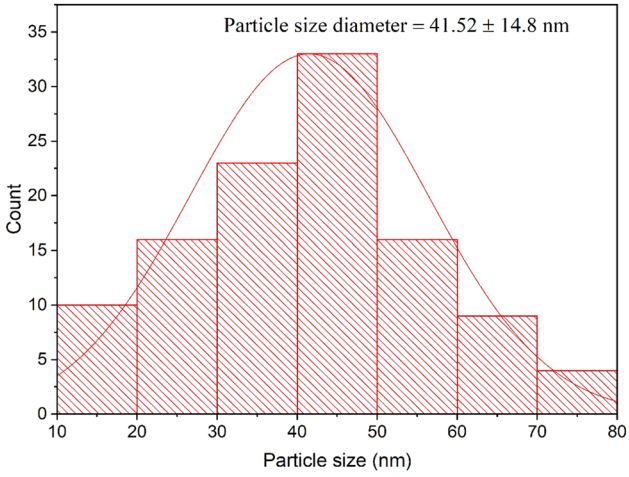

Figure 5: Particle size distribution histogram of the biogenic IONPs.

context, the C peak at 0.3 keV signal might be traced to the carbon tape employed during sample processing [50]. The elemental percentage of elemental iron was higher than that observed in a recent study that established the green synthesis of IONPs utilizing the *Ficus carica* (common fig) dried fruit extract with a relative elemental mass percentage of iron of 8.46% [51]. However, a recent study found that the proportion of elemental iron was 77.08%, which was substantially higher than that in our analysis [52]. This might be explained by the presence of another peak corresponding to the carbon element, which is attributed to the carbon tape.

3.5 FTIR spectrum of NPs

FTIR spectroscopy was used to identify the chemical groups present in NPs, with the aim of elucidating the main reducing, capping, and stabilizing agents. FTIR spectra revealed the presence of 14 distinct absorption peaks at certain wavenumbers. These peaks were observed at 3411.75, 2923.55, 1692.28, 1627.41, 1522.30, 1451.55, 1364.60, 1215.10, 1145.71, 1078.98, 1022.50, 826.27, 764.10, and 524.59 cm^{-1}, as visually shown in Figure 7. The absorption peak observed at 3411.75 cm^{-1} is attributed to the O–H stretching of alcohols, whereas the absorption band observed at 2923.55 cm^{-1} is associated with the C–H stretching of alkanes [53,54]. Moreover, the absorption peak at 1692.28 cm^{-1} was allocated to C═O stretching of aldehydes, while the band observed at 1627.41 cm^{-1} was accredited to C═C stretching of alkenes [55,56]. The spectral peak observed at 1522.30 cm^{-1} might be accredited to the stretching of N–O bonds in nitro compounds. Conversely, the spectral peak detected at 1451.55 cm^{-1} might be credited to the bending vibrations of C–H bonds in the CH_2 groups (Table 1) [57,58]. Furthermore, the medium

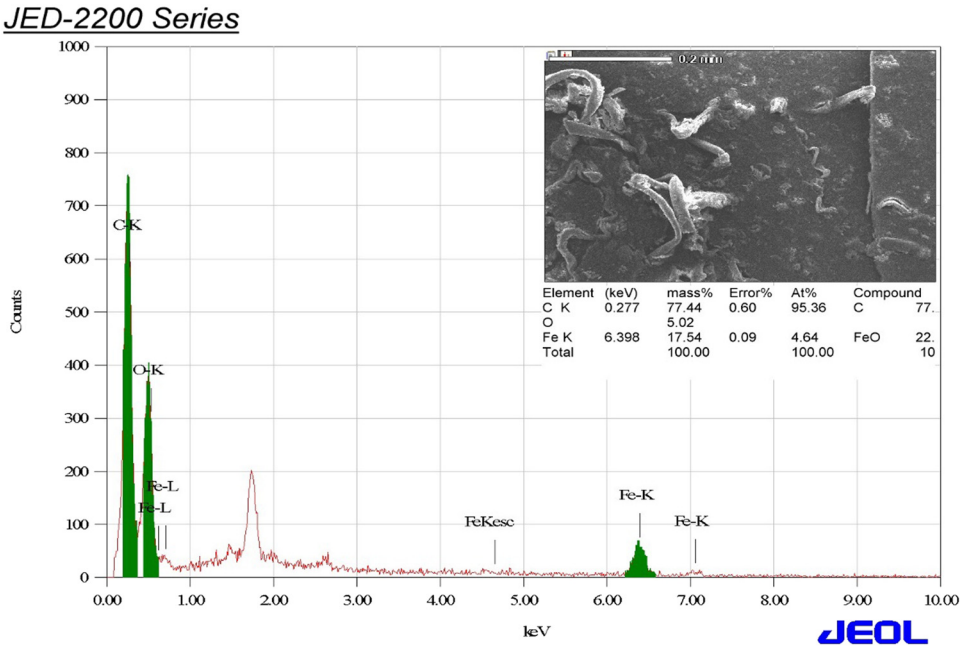

Figure 6: EDX spectrum of the biogenic IONPs.

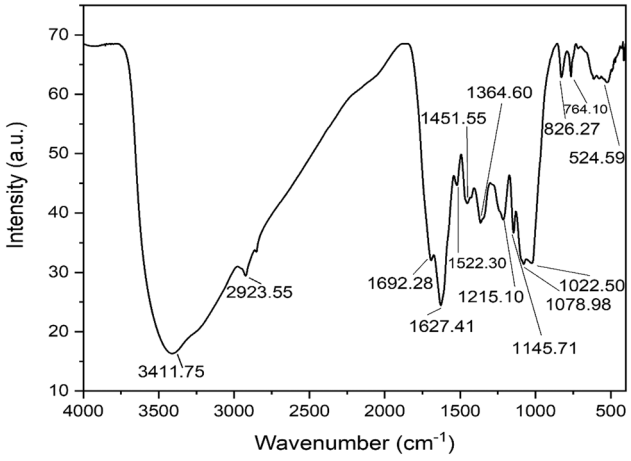

Figure 7: FTIR spectrum of the biogenic IONPs.

absorption band at 1215.10 cm^{-1} could be attributed to the C–N stretching of amines [59], whereas the peak observed at a wavenumber of 1,145 cm^{-1} corresponds to the anti-symmetric stretching of the C–O–C bridge [60]. Additionally, a band detected at 1,078 cm^{-1} may be attributed to the stretching of the C–O bond in primary alcohols [53]. On the other hand, the band detected at 1022.50 cm^{-1} could be allotted to the amines functional group [61]. The observed peak at 826.27 cm^{-1} might be ascribed to the bending motion of the carbon–carbon double bond (C═C) present in alkenes [62]. Furthermore, the band at 764.10 cm^{-1} might be ascribed to the C–Cl bond of halo compounds [63]. Finally, a band at 524 cm^{-1} in the IR pattern showed the Fe–O stretches of Fe_2O_3 and Fe_3O_4 compounds [64].

3.6 Zeta potential analysis

The eco-friendly prepared NPs demonstrated a diameter of 681.4 nm, as determined by dynamic light scattering (DLS) measurements (Figure 8). Additionally, the average surface charge of NPs was detected to be −5.48 mV, as presented in Figure 9. In this context, it is observed that the hydrodynamic diameter of the biogenic IONPs is greater than that determined through TEM and XRD analysis. This discrepancy arises from the fact that the DLS technique used for measurements takes into account not only the particle size of the biogenic IONPs but also includes the contribution from the surrounding capping molecules and additional hydrated layers that envelop the biogenic IONPs [65]. The negative zeta potential value of NPs might be ascribed to the presence of capping biomolecules, such as polyphenolic compounds, as reported in a prior study [66].

3.7 XRD analysis of the biogenic IONPs

XRD investigation of the biogenic NPs showed the presence of six diffraction peaks at 2θ degrees of 31.43, 35.03, 42.51, 52.46, 56.53, and 64.11° corresponding to Bragg reflections

Table 1: Functional groups of biogenic IONPs synthesized using the flower extract of *H. sabdariffa* L.

No.	Absorption peak (cm^{-1})	Appearance	Functional groups	Molecular motion
1	3411.75	Strong, broad	Alcohols	O–H stretching
2	2923.55	Medium	Alkanes	C–H stretching
3	1692.28	Medium	Conjugated aldehyde	C═O stretching
4	1627.41	Medium	Alkenes	C–H stretching
5	1522.30	Medium	Nitro compounds	N–O stretching
6	1451.55	Medium	Alkanes	C–H bending
7	1364.60	Medium	Phenols	O–H bending
8	1215.10	Medium	Amines	C–N stretching
9	1145.71	Medium	Alcohols	C–O–C stretching
10	1078.98	Medium	Primary alcohols	C–O stretching
11	1022.50	Medium	Amines	C–N stretching
12	826.27	Weak	Alkenes	C═C bending
13	764.10	Weak	Halo compounds	C–Cl stretching
14	524.59	Weak, broad	Metal oxides	Fe–O stretching

of 220, 311, 400, 422, 511, and 440, respectively (Figure 10). The outcomes of our investigation align with those of a preceding report, which proved the green production of biogenic IONPs using a water-based extract derived from *Hibiscus sabdariffa* flowers. The diffraction peaks observed at 2θ degrees of 31, 34, 42, 52, 56, and 64° corresponded to the Bragg reflections of (220), (311), (400), (422), (511), and (440), respectively [67]. Moreover, the biogenic IONPs synthesized using the extract of *Phoenix dactylifera* L. revealed the presence of six diffraction peaks at 2θ degrees of 30.25, 35.45,43.20, 53.39, 57.26, and 62.90° corresponding to the planes of (220), (311), (400), (422), (511), and (440), respectively [68]. Moreover, the prominent diffraction peaks reported in a prior report at 2θ angles of 30.2°, 35.7°, 43.2°, 53.7°, 57.1°, and 62.7° correspond to the diffraction of Fe_3O_4 crystal planes with Miller indices of (220), (311), (400), (422), (511), and (440) [69]. The diffraction peaks observed correspond precisely to the magnetic cubic structure of Fe_3O_4, as documented in the card number of JCPDS 65-3107 [70]. The crystalline size was calculated by Scherrer's formula: $D = (k\lambda/\beta\cos\theta)$, where λ represents the wavelength of X-ray (1.54178 Å), k is Scherer's constant (k = 0.94), θ is the diffraction angle (34.98°), and β is the full width at half-maximum (FWHM) of the most intense diffraction peak, which was measured to be 0.2584. The size of the crystals was determined to be 33.68 nm.

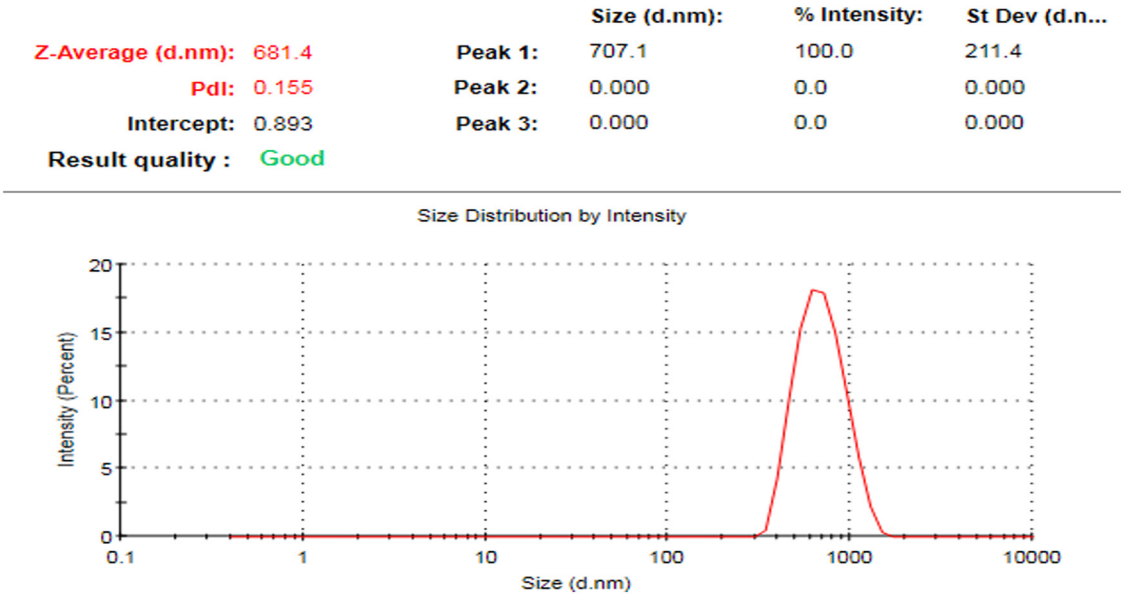

Figure 8: Average hydrodynamic diameter of the biogenic IONPs.

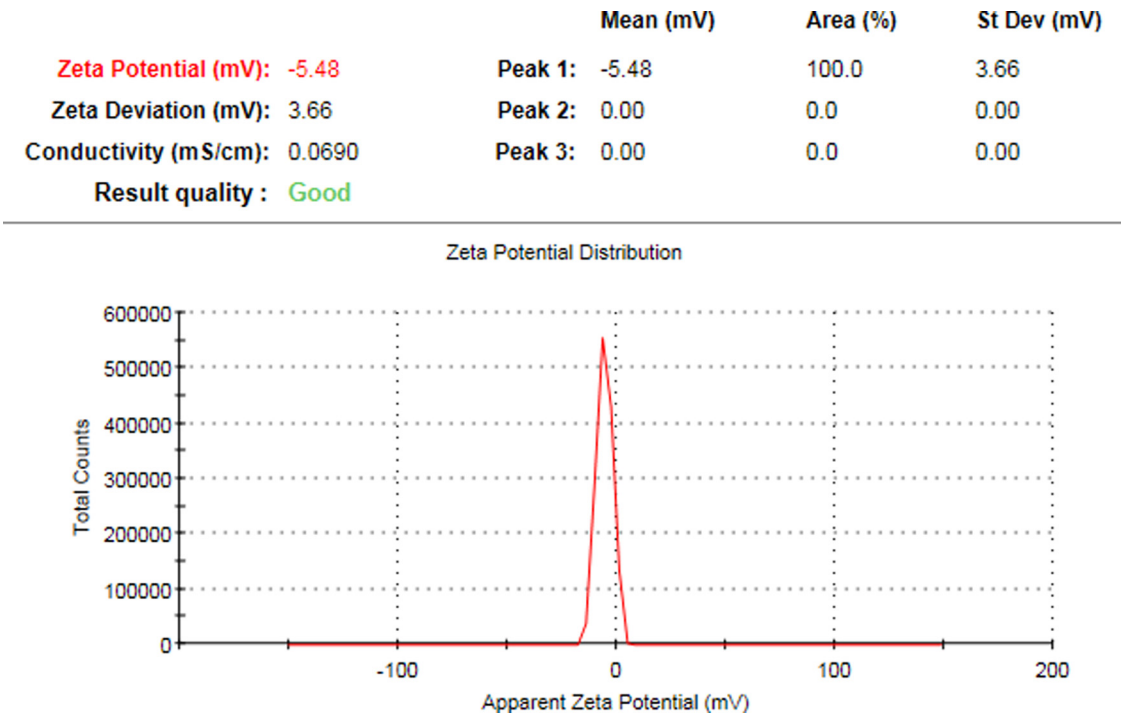

Figure 9: Surface charge of the biogenic IONPs.

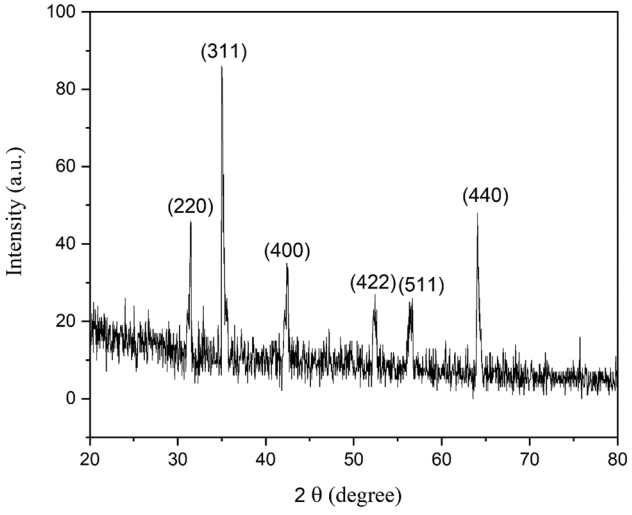

Figure 10: XRD spectrum of the biogenic IONPs.

3.8 Photocatalytic removal of rhodamine B using IONPs

The degradation percentage of rhodamine B dye was examined under dark and sunlight conditions in the presence of varied concentrations of the greenly produced IONPs. The degradation percentage of rhodamine B dye was examined at various doses of biogenic IONPs (0.5, 1.0, 2.0, and 4.0 mg/ml) and at varied reaction periods (30.0, 60.0, 90.0, 120.0, 150.0, 180.0, and 210.0 min). The degradation % of rhodamine B dye is dependent on both time and concentration. The decolorization percentage of rhodamine B dye was observed to vary between 10.52 and 46.21% under sunlight conditions at a concentration of 0.5 mg/ml of IONPs. This variation occurred at contact times of 30 and 210 min, respectively. Conversely, under dark conditions, the degradation percentage ranged from 4.43 to 11.97% at contact times of 30 and 210 min, respectively (Figure 11). In this context, IONPs exhibited limited effectiveness in decolorizing the rhodamine B dye at concentrations of 0.5 and 4.0 mg/ml. Even after a reaction time of 210 min, the decolorization efficiency remained relatively low, with degradation percentages of 11.97 and

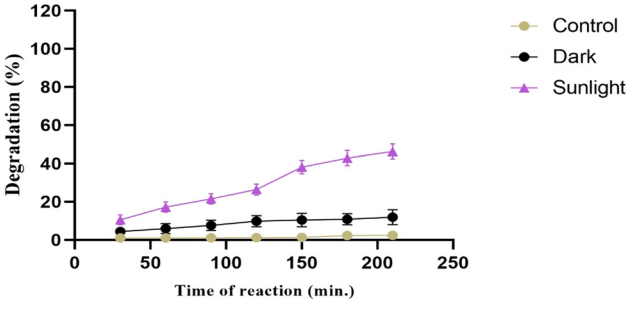

Figure 11: Percentage of rhodamine B removal under sunlight irradiation and at 0.5 mg/ml biogenic IONPs.

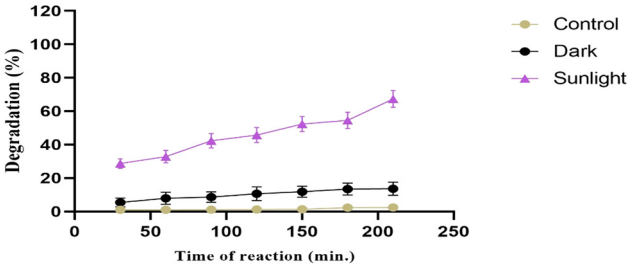

Figure 12: Percentage of rhodamine B removal under sunlight irradiation and at 1.0 mg/ml biogenic IONPs.

21.54% for the corresponding quantities, respectively. Our results align with those of Rajendran et al., who demonstrated that the photocatalytic efficacy did not show any improvement in the absence of visible light irradiation, even in the presence of a catalyst, and even after a reaction duration of 50 min [71]. In addition, the biogenic IONPs (1.0 mg/ml) exhibited low degradation efficiency ranging from 5.43 to 13.62% in the absence of light, with contact times ranging from 30 to 210 min, respectively. However, when exposed to sunlight, the removal efficiency significantly increased to 67.37% after a reaction time of 210 min (Figure 12). Furthermore, the biogenic IONPs at a concentration of 2.0 mg/ml exhibited a notable capacity for degrading rhodamine B dye when exposed to sunlight. The elimination percentages ranged from 38.15 to 77.37% for contact durations of 30 and 210 min, respectively (Figure 13). On the other hand, the IONP concentration of 4.0 mg/ml had the maximum photocatalytic activity, resulting in relative degradation percentages ranging from 39.17 to 92.46% at contact durations of 30 and 210 min, respectively, under sunlight conditions (Figure 14). In this context, increasing the dosage of IONPs synthesized using the papaya (*Carica papaya*) leaf extract improved dye decolorization, with a maximum of 76.6% occurring at pH 2 after 6 h at a catalyst concentration of 0.8 mg/ml [72]. The decolorization of the dye in our

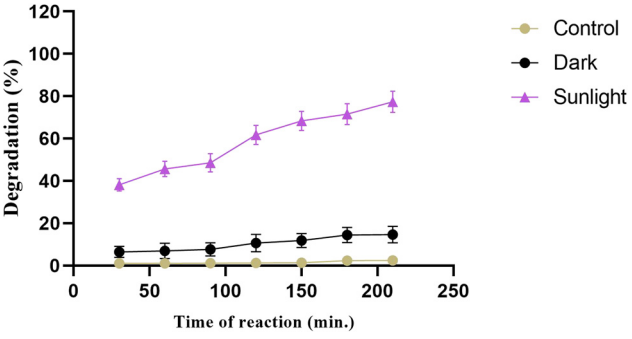

Figure 13: Percentage of rhodamine B removal under sunlight irradiation and at 2.0 mg/ml biogenic IONPs.

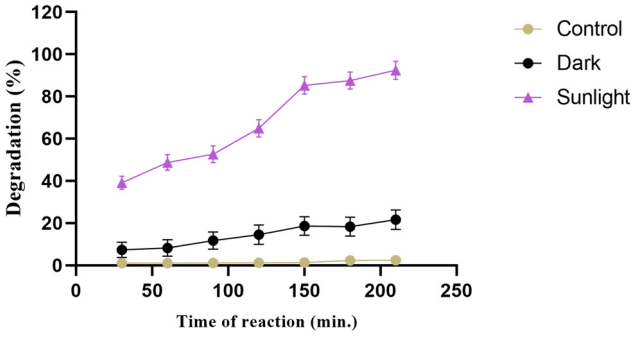

Figure 14: Percentage of rhodamine B removal under sunlight irradiation and at 4.0 mg/ml biogenic IONPs.

current study was greater than that in the previous report. This can be attributed to the higher concentration of biogenic IONPs, which was 4 mg/ml compared to the previous concentration of 0.8 mg/ml. This suggests that increasing the dosage of biogenic IONPs is effective in removing organic dyes. Moreover, the outcomes of our investigation line up with prior research that confirmed the effectiveness of IONPs in the photocatalytic degradation of rhodamine B dye. The previous report indicated that 92% of the rhodamine B dye molecules can be completely degraded through photodegradation within a 50-min timeframe. This degradation process was achieved using 50 mg of Fe_2O_3 NPs, which were synthesized using an environmentally friendly method involving the extract of *Cocos nucifera* L. [71]. Another investigation affirmed the efficiency of IONPs synthesized using the extract of *Dimocarpus longan* in a dramatic degradation of different dyes such as malachite green, CR, eosin-Y methylene blue, and rhodamine B [73]. The green synthesis of unique iron oxide particles was achieved by using the *Peltophorum pterocarpum* leaf extract in a previous study. These particles were then used for the photocatalytic and catalytic removal of rhodamine B from water. The results showed a high removal efficiency of 95% within a 60-min timeframe when subjected to UV irradiation [74]. Recent research has shown that the biogenic IONPs, which were synthesized using an extract derived from *Aegle marmelos*, had a degradation efficiency of 95.89% for Brilliant green dye for a duration of 90 min when subjected to UV light irradiation [75]. Previous research has shown that IONPs derived from the green tea leaf extract consist of iron oxide and oxohydroxide. In aqueous media, these catalysts have been used to remove organic dyes, such as methylene blue and methyl orange, in a manner similar to that of Fenton catalysts. Moreover, the study has shown considerable efficacy of these substances in the elimination of both cationic and anionic dyes over a broad spectrum of concentrations, ranging from 10 to 200 mg/l. Additionally, it has been shown

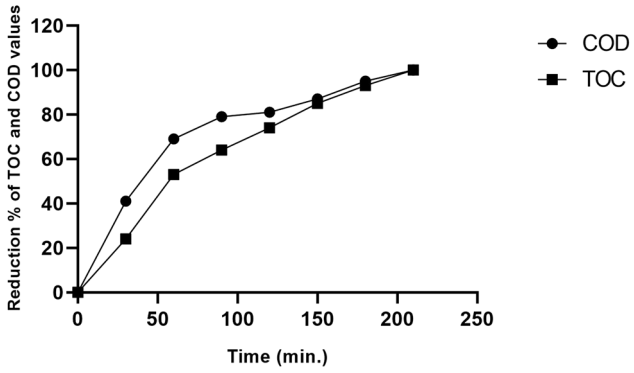

Figure 15: Reduction in TOC and COD values after photocatalytic degradation of the rhodamine B dye.

that IONPs synthesized using green tea leaf extract exhibit higher efficacy compared to those synthesized using borohydride reduction [76]. The collective evidence suggests that the biogenic IONPs have shown notable efficacy in the elimination of organic dyes when exposed to UV light, which is consistent with the results of the present investigation.

3.9 Investigation of degradation products

In order to verify the mineralization of the dye, a photocatalytic degradation process was conducted for a duration of 210 min. The samples that were exposed to sunlight irradiation were then analyzed using both COD and TOC methods. The findings indicated a complete elimination of COD and TOC levels when exposed to sunlight irradiation (Figure 15). It is noteworthy that the COD level declines at a somewhat quicker rate than the TOC level for Rh B, suggesting that the dye undergoes direct mineralization.

The degradation and mineralization degree was also monitored using HPLC analysis. The HPLC chromatograms demonstrate the breakdown of the pollutant into smaller pieces, which are then totally converted into minerals. An intense peak of the dye was found at 0 h of irradiation, whereas only 49% was recorded after 1 h of photocatalytic degradation. After 2 h of irradiation, the dye peak exhibited a significant reduction (approximately 65% reduction), and small additional peaks were identified at various retention times, indicating the presence of degradation products.

3.10 Mechanism of photocatalytic degradation of rhodamine B dye

The biogenic IONPs generate hydroxyl radicals (OH˙) when exposed to sunshine radiation. These radicals are responsible for breaking down the rhodamine B dye. The potential degradation process is shown in Figure 16. Typically, when NPs were exposed to sunlight, it resulted in the generation of an electron (e^-) and a hole (h+) pair [77]. The generated electron undergoes excitation, transitioning from the valence band to the conduction band, while the h+ remains in the valence band [78]. The presence of this hole (h+) facilitates the transformation of water into hydroxyl radical, which in turn leads to the oxidative breakdown of

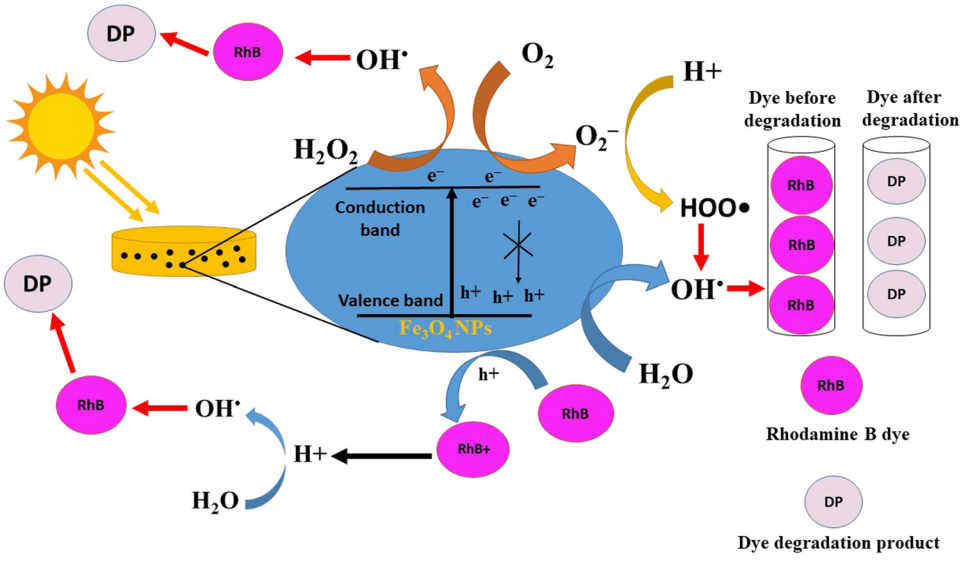

Figure 16: Mechanism of photocatalytic degradation of rhodamine B dye utilizing biogenic IONPs under sunlight irradiation.

Table 2: Antifungal activity of standard fungicide (metalaxyl + mancozeb) against the tested strains

Metalaxyl + mancozeb (ppm)	Fungal growth diameter (mm)		Growth inhibition Percentage (%)	
	P. digitatum ON201443	*A. niger* ON197883	ON201443	ON197883
Control (0 ppm)	58.13 ± 0.32[a]	79.12 ± 0.18[a]	0.00[a]	0.00[a]
50	51.23 ± 0.18[b]	61.24 ± 0.39[b]	11.87[b]	22.59[b]
100	46.23 ± 0.17[c]	52.46 ± 0.25[c]	20.47[c]	33.70[c]
200	31.64 ± 0.23[d]	43.17 ± 0.28[d]	45.57[d]	45.44[d]
400	26.18 ± 0.14[e]	35.26 ± 0.13[e]	54.96[e]	55.43[e]
800	20.16 ± 0.38[f]	32.41 ± 0.42[f]	65.32[f]	59.04[f]

Different superscript letters indicated that the values were significantly different.

dye [79]. Conversely, electrons react with molecular oxygen and are transformed into superoxide radicals. The superoxide radical undergoes further conversion into the hydroxyl radical, which has strong oxidizing properties and breaks down the dye into non-hazardous end products [80]. Once again, the very oxidizing vacancy created by NPs upon absorbing sunlight leads to the direct oxidation of dyes and the release of H+ ions. These ions then combine with water to form reactive oxygen species and OH^- ions, which aid in the breakdown of the dye [81]. In addition, the biomolecules found in the *H. sabdariffa* flower extract and on the surface of NPs serve as catalysts to enhance the photocatalytic activity and facilitate the enhanced breakdown of dye molecules [82].

3.11 Antifungal efficiency of the biogenic IONPs against fungal strains

The metalaxyl + mancozeb fungicide was more effective against *P. digitatum* ON201443 than *A. niger* ON197883, with relative inhibition percentages of 65.32 and 59.04%, respectively (Table 2). In contrast, biogenic IONPs at 800 ppm had more antifungal efficacy against *A. niger* ON197883 than *P. digitatum* ON201443, with relative inhibition percentages of 81.87 and 78.54%, respectively (Table 3). The biogenic IONPs, prepared using the extract from the leaves of *Platanus orientalis*, were shown to have antifungal properties against *Mucor piriformis* and *A. niger* [83]. These results align with our findings. Koka et al. confirmed the same results, reporting that IONPs have antifungal properties against rot-causing fungi such as *A. niger*, *Penicillium expansum*, and *Penicillium chrysogenum* strains [84]. In addition, the biogenic Fe_3O_4-NPs derived from *Colpomenia sinuosa* showed remarkable antifungal activity against *A. flavus* and *F. oxysporum* strains [85]. Furthermore, the biogenic IONPs produced using extracts from *Aegle marmelos* had a greater antifungal effect against the *Fusarium solani* strain compared to the fluconazole antifungal agent at a dose of 30 µg/ml [75]. Furthermore, the biogenic iron NPs showed superior effectiveness in inhibiting the growth of *A. niger* and *P. digitatum* strains compared to the conventional fungicide metalaxyl + mancozeb when tested at the same doses. The notable antifungal efficacy of the biogenic IONPs, in comparison to conventional fungicides, indicates the possible use of these environmentally friendly synthesized NPs in the development of natural fungicides. This would help mitigate the detrimental impact of continuous usage of chemical fungicides on the environment [86]. The

Table 3: Antifungal efficiency of the biogenic IONPs against fungal pathogens

Biogenic IONPs (ppm)	Fungal growth diameter (mm)		Growth inhibition Percentage (%)	
	P. digitatum ON201443	*A. niger* ON197883	ON201443	ON197883
Control (0 ppm)	59.45 ± 0.19[a]	79.32 ± 0.21[a]	0.00[a]	0.00[a]
50	43.12 ± 0.26[b]	57.34 ± 0.53[b]	27.46[b]	27.71[b]
100	31.67 ± 0.25[c]	46.18 ± 0.34[c]	46.73[c]	41.02[c]
200	21.18 ± 0.45[d]	36.29 ± 0.16[d]	64.37[d]	54.25[d]
400	17.23 ± 0.34[e]	26.13 ± 0.27[e]	71.02[e]	67.08[e]
800	12.76 ± 0.51[f]	14.38 ± 0.38[f]	78.54[f]	81.87[f]

Different superscript letters indicated that the values were significantly different.

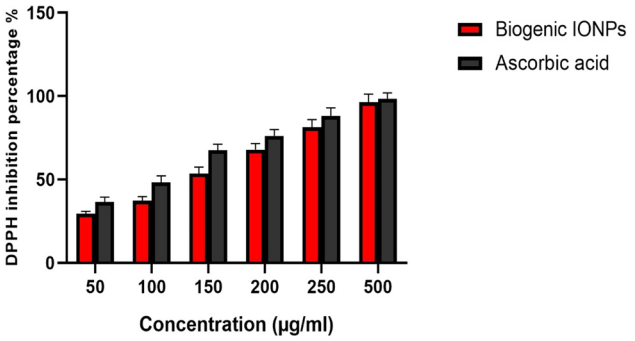

Figure 17: DPPH inhibition percentages (%) of biogenic IONPs.

biogenic iron NPs' antifungal effectiveness can be ascribed to their significant surface-to-volume ratio, which enables them to adhere tenaciously to the fungal cell surface [87]. Additionally, owing to its diminutive dimensions, it is capable of immediately infiltrating the cell and causing disruption to its protective barrier [88]. The inactivation of fungus by IONPs occurs via a direct contact between the NPs and the surfaces of the fungal cells [89]. This interaction changes the permeability of the cell membranes, allowing the NPs to penetrate and create oxidative stress inside the fungal cells [90]. As a consequence, the development of the cells is inhibited, finally leading to their death. The literature has described the potential for membrane damage resulting from direct or electrostatic contact between IONPs and cell surfaces, as well as cellular internalization of NPs. Additionally, the formation of active oxygen species, such as H_2O_2, in cells owing to metal oxides has also been shown [91]. The biogenic IONPs demonstrated relative MIC values of 0.125 and 0.250 mg/ml against *P. digitatum* and *A. niger* strains, respectively. A prior study demonstrated the use of tannic acid in an alkaline solution to synthesize biogenic IONPs. These IONPs showed a relative MIC value of 0.016 mg/ml against the strains of *A. niger* and *P. chrysogenum* [45]. Hematite (α-Fe_2O_3) NPs synthesized utilizing *A. niger* showed antifungal properties against the *Aspergillus fumigatus* strain, with a relative MIC value of 62.5 µg/ml [92]. Another report indicated the green fabrication of IONPs using the leaf extract of *Rhamnus virgata*, demonstrating a relative MIC value of 125 µg/ml against *Aspergillus flavus*, whereas the MIC value of the biogenic IONPs against *Mucor racemosus*, *A. niger,* and *Fusarium solani* was 31.25 µg/ml [93]. The difference in MIC values between our findings and previous reports might be attributed to the utilization of different biological sources in the synthesis process of the biogenic IONPs. Different biological sources might have varying capping agents adsorbed onto the surface of the biogenic IONPs, leading to different antifungal activity patterns against the tested pathogens.

3.12 Antioxidant assay

The DPPH inhibition percentages were measured for various doses of biogenic IONPs, extending from 50 to 500 mg/ml, and compared to ascorbic acid. In this regard, biogenic IONPs exhibited DPPH inhibition percentages of 29.43 and 96.35% at concentrations of 50 and 500 mg/ml, respectively (Figure 17). The biogenic IONPs fabricated using the *H. sabdariffa* flower extract exhibited an IC_{50} value of 139.87 mg/ml, whereas the standard ascorbic acid demonstrated a relative IC_{50} of 103.14 mg/ml. Thus, it is suggested that biogenic IONPs may eliminate free radicals by either transferring hydrogen atoms or contributing electrons to DPPH radicals. Consequently, it may stop the process of oxidation and protect proteins, nucleic acids, carbohydrates, and lipids from oxidative damage [94]. Hence, the prospective antioxidant capability of IONPs has promise as a means of combating cancer and other harmful diseases in the future.

4 Conclusions

The biogenic IONPs demonstrated potential photocatalytic activity against the rhodamine B dye, and the photocatalytic activity was concentration- and time-dependent. In this context, the highest rhodamine B removal percentage was detected at a concentration of 4.0 mg/ml of biogenic IONPs under sunlight illumination after a 210.0-min reaction period. Furthermore, the biogenic IONPs exhibited superior effectiveness in inhibiting the growth of the tested fungal strains compared to the fungicide metalaxyl + mancozeb. This emphasizes the potential use of these nanomaterials in managing fungal phytopathogens as non-toxic substitutes for chemical fungicides. Moreover, the efficient antioxidant activity of the biogenic IONPs emphasizes their prospective usage for biomedical applications.

Acknowledgments: The author would like to thank the King Khalid Military Academy, Riyadh, Saudi Arabia, for the technical support for this research.

Funding information: This research was funded by King Khalid Military Academy, Riyadh, Saudi Arabia.

Author contributions: K.M.: investigation, data curation, analysis, writing original draft and writing, reviewing and editing of the final version.

Conflict of interest: The author declares no conflict of interest.

Data availability statement: All data generated or analyzed during this study are included in this published article and its supplementary information files.

References

[1] Mukhopadhyay A, Duttagupta S, Mukherjee A. Emerging organic contaminants in global community drinking water sources and supply: A review of occurrence, processes and remediation. J Environ Chem Eng. 2022 Jun;10(3):107560.

[2] Fida M, Li P, Wang Y, Alam SMK, Nsabimana A. Water contamination and human health risks in Pakistan: A review. Expo Health. 2022;15:619–39. doi: 10.1007/s12403-022-00512-1.

[3] Inyinbor Adejumoke A, Adebesin Babatunde O, Oluyori Abimbola P, Adelani Akande Tabitha A, Dada Adewumi O, Oreofe Toyin A. Water pollution: effects, prevention, and climatic impact. Water Chall Urban World. 2018;33:33–47.

[4] Chowdhary P, Bharagava RN, Mishra S, Khan N. Role of industries in water scarcity and its adverse effects on environment and human health. In: Shukla V, Kumar N, editors. Environmental concerns and sustainable development: Volume 1: Air, water and energy resources [Internet]. Singapore: Springer; 2020. p. 235–56. [cited 2023 Jul 31]. doi: 10.1007/978-981-13-5889-0_12.

[5] Al-Gheethi AA, Azhar QM, Senthil Kumar P, Yusuf AA, Al-Buriahi AK, Radin Mohamed RMS, et al. Sustainable approaches for removing Rhodamine B dye using agricultural waste adsorbents: A review. Chemosphere. 2022 Jan;287:132080.

[6] Abdelrahman EA, Al-Farraj ES. Facile synthesis and characterizations of mixed metal oxide nanoparticles for the efficient photocatalytic degradation of Rhodamine B and Congo Red Dyes. Nanomaterials. 2022 Jan;12(22):3992.

[7] Kumar S, Yadav S, Kataria N, Chauhan AK, Joshi S, Gupta R, et al. Recent advancement in nanotechnology for the treatment of pharmaceutical wastewater: Sources, toxicity, and remediation technology. Curr Pollut Rep. 2023 Jun;9(2):110–42.

[8] Dave S, Das J, Varshney B, Sharma VP. Dyes and pigments: Interventions and how safe and sustainable are colors of life!!! In: Dave S, Das J, editors. Trends and contemporary technologies for photocatalytic degradation of dyes [Internet]. Cham: Springer International Publishing; 2022. p. 1–20. [cited 2024 Feb 14]. (Environmental Science and Engineering). doi: 10.1007/978-3-031-08991-6_1.

[9] Tkaczyk A, Mitrowska K, Posyniak A. Synthetic organic dyes as contaminants of the aquatic environment and their implications for ecosystems: A review. Sci Total Env. 2020 May;717:137222.

[10] Kishor R, Purchase D, Saratale GD, Saratale RG, Ferreira LFR, Bilal M, et al. Ecotoxicological and health concerns of persistent coloring pollutants of textile industry wastewater and treatment approaches for environmental safety. J Env Chem Eng. 2021 Apr;9(2):105012.

[11] Saravanan A, Senthil Kumar P, Jeevanantham S, Karishma S, Tajsabreen B, Yaashikaa PR, et al. Effective water/wastewater treatment methodologies for toxic pollutants removal: Processes and applications towards sustainable development. Chemosphere. 2021 Oct;280:130595.

[12] Misra M, Akansha K, Sachan A, Sachan SG. Removal of dyes from industrial effluents by application of combined biological and physicochemical treatment approaches. In: Shah M, Banerjee A, editors. Combined application of physico-chemical & microbiological processes for industrial effluent treatment plant [Internet]. Singapore: Springer; 2020. p. 365–407. [cited 2024 Feb 14]. doi: 10.1007/978-981-15-0497-6_17

[13] Roy M, Saha R. 6 - Dyes and their removal technologies from wastewater: A critical review. In: Bhattacharyya S, Mondal NK, Platos J, Snášel V, Krömer P, editors. Intelligent environmental data monitoring for pollution management [Internet]. Academic Press; 2021. p. 127–60. (Intelligent Data-Centric Systems). [cited 2024 Feb 14]. https://www.sciencedirect.com/science/article/pii/B9780128196717000063.

[14] Tripathi S, Hussain T. Chapter 7 – Water and Wastewater Treatment through Ozone-based technologies. In: Shah M, Rodriguez-Couto S, Biswas J, editors. Development in wastewater treatment research and processes [Internet]. Elsevier; 2022. p. 139–72. [cited 2024 Feb 14]. https://www.sciencedirect.com/science/article/pii/B9780323855839000156.

[15] Gautam S, Agrawal H, Thakur M, Akbari A, Sharda H, Kaur R, et al. Metal oxides and metal organic frameworks for the photocatalytic degradation: A review. J Env Chem Eng. 2020 Jun;8(3):103726.

[16] Mancuso A, Blangetti N, Sacco O, Freyria FS, Bonelli B, Esposito S, et al. Photocatalytic degradation of crystal violet dye under visible light by Fe-Doped TiO2 Prepared by reverse-micelle sol–gel method. Nanomaterials. 2023 Jan;13(2):270.

[17] Mishra S, Sundaram B. A review of the photocatalysis process used for wastewater treatment. Mater Today Proc. 2023;234:349. https://www.sciencedirect.com/science/article/pii/S2214785323040166.

[18] Yang H, He D, Liu C, Zhou X, Qu J. Magnetic photocatalytic antimicrobial materials for water disinfection. Sep Purif Technol. 2023;325:124697.

[19] Pandey AK, Reji Kumar R, Kalidasan B, Laghari IA, Samykano M, Kothari R, et al. Utilization of solar energy for wastewater treatment: Challenges and progressive research trends. J Environ Manage. 2021 Nov;297:113300.

[20] Davies KR, Cherif Y, Pazhani GP, Anantharaj S, Azzi H, Terashima C, et al. The upsurge of photocatalysts in antibiotic micropollutants treatment: Materials design, recovery, toxicity and bioanalysis. J Photochem Photobiol C Photochem Rev. 2021 Sep;48:100437.

[21] Joudeh N, Linke D. Nanoparticle classification, physicochemical properties, characterization, and applications: A comprehensive review for biologists. J Nanobiotechnology. 2022;20(1):262.

[22] Sharma N, Ojha H, Bharadwaj A, Pathak DP, Sharma RK. Preparation and catalytic applications of nanomaterials: A review. Rsc Adv. 2015;5(66):53381–403.

[23] Alharbi NS, Alsubhi NS, Felimban AI. Green synthesis of silver nanoparticles using medicinal plants: Characterization and application. J Radiat Res Appl Sci. 2022;15(3):109–24.

[24] Seabra AB, Haddad P, Duran N. Biogenic synthesis of nanostructured iron compounds: applications and perspectives. IET Nanobiotechnol. 2013;7(3):90–9.

[25] Chavali MS, Nikolova MP. Metal oxide nanoparticles and their applications in nanotechnology. SN Appl Sci. 2019 May;1(6):607.

[26] Thangavelu L, Veeraragavan GR, Mallineni SK, Devaraj E, Parameswari RP, Syed NH, et al. Role of nanoparticles in environmental remediation: An insight into heavy metal pollution from dentistry. Bioinorg Chem Appl. 2022 Mar;2022:e1946724.

[27] Qumar U, Hassan JZ, Bhatti RA, Raza A, Nazir G, Nabgan W, et al. Photocatalysis vs adsorption by metal oxide nanoparticles. J Mater Sci Technol. 2022;131:122–66.
[28] Ali A, Zafar H, Zia M, ul Haq I, Phull AR, Ali JS, et al. Synthesis, characterization, applications, and challenges of iron oxide nanoparticles. Nanotechnol Sci Appl. 2016 Aug;9:49–67.
[29] Muthukumar H, Matheswaran M. Amaranthus spinosus leaf extract mediated FeO nanoparticles: physicochemical traits, photocatalytic and antioxidant activity. ACS Sustain Chem Eng. 2015;3(12):3149–56.
[30] Alagiri M, Hamid SBA. Green synthesis of α-Fe2O3 nanoparticles for photocatalytic application. J Mater Sci Mater Electron. 2014 Aug;25(8):3572–7.
[31] Priyan VV, Kumar N, Narayanasamy S. Toxicological assessment and adsorptive removal of lead (Pb) and Congo red (CR) from water by synthesized iron oxide/activated carbon (Fe3O4/AC) nanocomposite. Chemosphere. 2022 May;294:133758.
[32] Jeyabalan J, Veluchamy A, VVP, Kumar A, Chandrasekar R, Narayanasamy S. A review on the laccase assisted decolourization of dyes: Recent trends and research progress. J Taiwan Inst Chem Eng. 2023 Oct;151:105081.
[33] Kumar A, Jeyabalan J, Priyan VV, Charan Patra C, Narayanasamy S. Fabrication of a novel bio-polymer adsorbent with high adsorptive capacity towards organic dyes. Ind Crop Prod. 2023 Nov;203:117166.
[34] Varadharaj VP, Ramesh G, Kumar A, Jeyabalan J, Narayanasamy S. Synthesis, characterization, and application of oxidant-modified biochar prepared from sawdust for sequestration of basic fuchsin: Isotherm, kinetics, and toxicity studies. Biomass Convers Biorefin. 2023 Jul;13(11):9525–36.
[35] Altuner EE, Gulbagca F, Tiri RNE, Aygun A, Sen F. Highly efficient palladium-zinc oxide nanoparticles synthesized by biogenic methods: Characterization, hydrogen production and photocatalytic activities. Chem Eng J Adv. 2023 May;14:100465.
[36] Yassin MT, Al-Otibi FO, Al-Askar AA, Alharbi RI. Green synthesis, characterization, and antifungal efficiency of biogenic iron oxide nanoparticles. Appl Sci. 2023 Jan;13(17):9942.
[37] Riaz G, Chopra R. A review on phytochemistry and therapeutic uses of Hibiscus sabdariffa L. Biomed Pharmacother. 2018 Jun;102:575–86.
[38] Cid-Ortega S, Guerrero-Beltrán JA. Roselle calyces (Hibiscus sabdariffa), an alternative to the food and beverages industries: A review. J Food Sci Technol. 2015 Nov;52(11):6859–69.
[39] Maciel LG, do Carmo MAV, Azevedo L, Daguer H, Molognoni L, de Almeida MM, et al. *Hibiscus sabdariffa* anthocyanins-rich extract: Chemical stability, *in vitro* antioxidant and antiproliferative activities. Food Chem Toxicol. 2018 Mar;113:187–97.
[40] Ali BH, Wabel NA, Blunden G. Phytochemical, pharmacological and toxicological aspects of Hibiscus sabdariffa L.: A review. Phytother Res. 2005;19(5):369–75.
[41] Izquierdo-Vega JA, Arteaga-Badillo DA, Sánchez-Gutiérrez M, Morales-González JA, Vargas-Mendoza N, Gómez-Aldapa CA, et al. Organic acids from Roselle (Hibiscus sabdariffa L.)—A brief review of its pharmacological effects. Biomedicines. 2020 May;8(5):100.
[42] Jamzad M, Kamari Bidkorpeh M. Green synthesis of iron oxide nanoparticles by the aqueous extract of Laurus nobilis L. leaves and evaluation of the antimicrobial activity. J Nanostruct Chem. 2020 Sep;10(3):193–201.
[43] Beheshtkhoo N, Kouhbanani MAJ, Savardashtaki A, Amani AM, Taghizadeh S. Green synthesis of iron oxide nanoparticles by aqueous leaf extract of Daphne mezereum as a novel dye removing material. Appl Phys A. 2018 Apr;124(5):363.
[44] Taha Yassin M, Al-Otibi FO, Al-Askar AA. Green synthesis, characterization and antimicrobial activity of iron oxide nanoparticles with tigecycline against multidrug resistant bacterial strains. J King Saud Univ – Sci. 2024 Apr;36(4):103131.
[45] Parveen S, Wani AH, Shah MA, Devi HS, Bhat MY, Koka JA. Preparation, characterization and antifungal activity of iron oxide nanoparticles. Microb Pathog. 2018 Feb;115:287–92.
[46] Wang X, Xu J, Wang X, Qiu B, Cuthbertson AGS, Du C, et al. Isaria fumosorosea-based zero-valent iron nanoparticles affect the growth and survival of sweet potato whitefly, Bemisia tabaci (Gennadius). Pest Manag Sci. 2019;75(8):2174–81.
[47] Xu B, Yang H, Cai Y, Yang H, Li C. Preparation and photocatalytic property of spindle-like MIL-88B(Fe) nanoparticles. Inorg Chem Commun. 2016 May;67:29–31.
[48] Abid MA, Kadhim DA. Novel comparison of iron oxide nanoparticle preparation by mixing iron chloride with henna leaf extract with and without applied pulsed laser ablation for methylene blue degradation. J Environ Chem Eng. 2020 Oct;8(5):104138.
[49] Zeeshan T, Obaid A, Waseem S, Danish Ali M, Kayani Z, Brahmia A. Investigation on structural, optical and anti-bacterial properties of organic additives iron oxide prepared by chemical route method. Arab J Chem. 2024 Feb;17(2):105581.
[50] Kannaujia R, Srivastava CM, Prasad V, Singh BN, Pandey V. Phyllanthus emblica fruit extract stabilized biogenic silver nanoparticles as a growth promoter of wheat varieties by reducing ROS toxicity. Plant Physiol Biochem. 2019 Sep;142:460–71.
[51] Aksu Demirezen D, Yıldız YŞ, Yılmaz Ş, Demirezen Yılmaz D. Green synthesis and characterization of iron oxide nanoparticles using *Ficus carica* (common fig) dried fruit extract. J Biosci Bioeng. 2019 Feb;127(2):241–5.
[52] Jagathesan G, Rajiv P. Biosynthesis and characterization of iron oxide nanoparticles using Eichhornia crassipes leaf extract and assessing their antibacterial activity. Biocatal Agric Biotechnol. 2018 Jan;13:90–4.
[53] Bayat M, Zargar M, Astarkhanova T, Pakina E, Ladan S, Lyashko M, et al. Facile biogenic synthesis and characterization of seven metal-based nanoparticles conjugated with phytochemical bioactives using Fragaria ananassa Leaf Extract. Molecules. 2021 Jan;26(10):3025.
[54] Sorbiun M, Shayegan Mehr E, Ramazani A, Taghavi Fardood S. Biosynthesis of Ag, ZnO and bimetallic Ag/ZnO alloy nanoparticles by aqueous extract of oak fruit hull (Jaft) and investigation of photocatalytic activity of ZnO and bimetallic Ag/ZnO for degradation of basic violet 3 dye. J Mater Sci Mater Electron. 2018 Feb;29(4):2806–14.
[55] Abou Baker DH, Abbas HS. Antimicrobial activity of biosynthesized Cuo/Se nanocomposite against Helicobacter pylori. Arab J Chem. 2023 Sep;16(9):105095.
[56] Majoumouo MS, Sharma JR, Sibuyi NRS, Tincho MB, Boyom FF, Meyer M. Synthesis of biogenic gold nanoparticles from terminalia mantaly extracts and the evaluation of their in vitro cytotoxic effects in cancer cells. Molecules. 2020 Jan;25(19):4469.
[57] Kaur G, Kaur H, Kumar S, Verma V, Jhinjer HS, Singh J, et al. Blooming approach: One-pot biogenic synthesis of TiO_2 nanoparticles using piper betle for the degradation of industrial reactive yellow 86 dye. J Inorg Organomet Polym Mater. 2021 Mar;31(3):1111–9.

[58] Del Buono D, Luzi F, Tolisano C, Puglia D, Di Michele A. Synthesis of a lignin/zinc oxide hybrid nanoparticles system and its application by nano-priming in maize. Nanomaterials. 2022 Jan;12(3):568.
[59] Ifeanyichukwu UL, Fayemi OE, Ateba CN. Green synthesis of zinc oxide nanoparticles from pomegranate (Punica granatum) extracts and characterization of their antibacterial activity. Molecules. 2020;25(19):4521.
[60] Hassan Afandy H, Sabir DK, Aziz SB. Antibacterial activity of the green synthesized plasmonic silver nanoparticles with crystalline structure against gram-positive and gram-negative bacteria. Nanomaterials. 2023 Jan;13(8):1327.
[61] Padmavathi J, Mani M, Gokulakumar B, Ramesh A, Anantharaj A, Kaviyarasu K. A study on the antibacterial activity of silver nanoparticles derived from Corchorus aestuans leaves and their characterization. Chem Phys Lett. 2022 Oct;805:139952.
[62] Eid AM, Fouda A, Niedbała G, Hassan SED, Salem SS, Abdo AM, et al. Endophytic Streptomyces laurentii mediated green synthesis of Ag-NPs with antibacterial and anticancer properties for developing functional textile fabric properties. Antibiotics. 2020 Oct;9(10):641.
[63] Dixit D, Gangadharan D, Popat KM, Reddy CRK, Trivedi M, Gadhavi DK. Synthesis, characterization and application of green seaweed mediated silver nanoparticles (AgNPs) as antibacterial agents for water disinfection. Water Sci Technol. 2018 Jul;78(1):235–46.
[64] Khan A, Afzal M, Rasool K, Ameen M, Qureshi NA. In-vivo anticoccidial efficacy of green synthesized iron-oxide nanoparticles using Ficus racemosa Linn leaf extract. (Moraceae) against Emeria tenella infection in broiler chickens. Vet Parasitol. 2023 Aug;110003.
[65] Rolim WR, Pelegrino MT, de Araújo Lima B, Ferraz LS, Costa FN, Bernardes JS, et al. Green tea extract mediated biogenic synthesis of silver nanoparticles: Characterization, cytotoxicity evaluation and antibacterial activity. Appl Surf Sci. 2019 Jan;463:66–74.
[66] Edison TJI, Sethuraman MG. Biogenic robust synthesis of silver nanoparticles using Punica granatum peel and its application as a green catalyst for the reduction of an anthropogenic pollutant 4-nitrophenol. Spectrochim Acta A Mol Biomol Spectrosc. 2013;104:262–4.
[67] Alshehri A, Ahmad Malik M, Khan Z, Ahmed Al-Thabaiti S, Hasan N. Biofabrication of Fe nanoparticles in aqueous extract of Hibiscus sabdariffa with enhanced photocatalytic activities. RSC Adv. 2017;7(40):25149–59.
[68] Abdullah JAA, Salah Eddine L, Abderrhmane B, Alonso-González M, Guerrero A, Romero A. Green synthesis and characterization of iron oxide nanoparticles by pheonix dactylifera leaf extract and evaluation of their antioxidant activity. Sustain Chem Pharm. 2020 Sep;17:100280.
[69] Shahriary M, Veisi H, Hekmati M, Hemmati S. In situ green synthesis of Ag nanoparticles on herbal tea extract (*Stachys lavandulifolia*)-modified magnetic iron oxide nanoparticles as antibacterial agent and their 4-nitrophenol catalytic reduction activity. Mater Sci Eng C. 2018 Sep;90:57–66.
[70] Yang J, Kou Q, Liu Y, Wang D, Lu Z, Chen L, et al. Effects of amount of benzyl ether and reaction time on the shape and magnetic properties of Fe3O4 nanocrystals. Powder Technol. 2017 Sep;319:53–9.
[71] Rajendran A, Alsawalha M, Alomayri T. Biogenic synthesis of husked rice-shaped iron oxide nanoparticles using coconut pulp (Cocos nucifera L.) extract for photocatalytic degradation of Rhodamine B dye and their in vitro antibacterial and anticancer activity. J Saudi Chem Soc. 2021 Sep;25(9):101307.
[72] Bhuiyan MdSH, Miah MY, Paul SC, Aka TD, Saha O, Rahaman MdM, et al. Green synthesis of iron oxide nanoparticle using *Carica papaya* leaf extract: application for photocatalytic degradation of remazol yellow RR dye and antibacterial activity. Heliyon. 2020 Aug;6(8):e04603.
[73] Yuan M, Fu X, Yu J, Xu Y, Huang J, Li Q, et al. Green synthesized iron nanoparticles as highly efficient fenton-like catalyst for degradation of dyes. Chemosphere. 2020 Dec;261:127618.
[74] Shah Y, Maharana M, Sen S. *Peltophorum pterocarpum* leaf extract mediated green synthesis of novel iron oxide particles for application in photocatalytic and catalytic removal of organic pollutants. Biomass Convers Biorefin. 2022;1–14. doi: 10.1007/s13399-021-02189-z.
[75] Sriramulu M, Balaji, Sumathi S. Photo catalytic, antimicrobial and antifungal activity of biogenic iron oxide nanoparticles synthesised using Aegle marmelos extracts. J Inorg Organomet Polym Mater. 2021 Apr;31(4):1738–44.
[76] Shahwan T, Abu Sirriah S, Nairat M, Boyacı E, Eroğlu AE, Scott TB, et al. Green synthesis of iron nanoparticles and their application as a Fenton-like catalyst for the degradation of aqueous cationic and anionic dyes. Chem Eng J. 2011 Aug;172(1):258–66.
[77] Gautam N, Bahadur Singh K, Snigdha, Dayal Upadhyay D, Pandey G. Structural and optical properties of silver supported α-Fe 2 O 3 nanocomposite fabricated by Saraca asoca leaf extract for the effective photodegradation of cationic dye Azure B. RSC Adv. 2023;13(33):23181–96.
[78] Yadav P, Dhariwal N, Kumari M, Kumar V, Thakur OP. Enhanced degradation of Congo-red dye by Cr3+ doped α-Fe2O3 nanoparticles under sunlight and industrial wastewater treatment. Chemosphere. 2023 Dec;343:140208.
[79] Wang F, Yu X, Ge M, Wu S, Guan J, Tang J, et al. Facile self-assembly synthesis of γ-Fe2O3/graphene oxide for enhanced photo-Fenton reaction. Env Pollut. 2019 May;248:229–37.
[80] Sah PM, Gite SG, Sonawane R, Raut RW. Biogenic nanomaterials as a catalyst for photocatalytic dye degradation. In: Shah MP, Bharadvaja N, Kumar L, editors. Biogenic nanomaterials for environmental sustainability: Principles, practices, and opportunities [Internet]. Cham: Springer International Publishing; 2024. p. 409–33. (Environmental Science and Engineering). [cited 2024 Feb 15] doi: 10.1007/978-3-031-45956-6_16.
[81] Yassin MT, Al-Otibi FO, Al-Askar AA. Photocatalytic removal of crystal violet dye utilizing greenly synthesized iron oxide nanoparticles. Separations. 2023 Sep;10(9):513.
[82] Haritha E, Roopan SM, Madhavi G, Elango G, Al-Dhabi NA, Arasu MV. Green chemical approach towards the synthesis of SnO2 NPs in argument with photocatalytic degradation of diazo dye and its kinetic studies. J Photochem Photobiol B. 2016 Sep;162:441–7.
[83] Devi HS, Boda MA, Shah MA, Parveen S, Wani AH. Green synthesis of iron oxide nanoparticles using Platanus orientalis leaf extract for antifungal activity. Green Process Synth. 2019 Jan;8(1):38–45.
[84] Koka JA, Wani AH, Bhat MY. Evaluation of antifungal activity of Magnesium oxide (MgO) and Iron oxide (FeO) nanoparticles on rot causing fungi. J Drug Deliv Ther. 2019 Apr;9(2–s):173–8.
[85] Salem DMSA, Ismail MM, Aly-Eldeen MA. Biogenic synthesis and antimicrobial potency of iron oxide (Fe3O4) nanoparticles using algae harvested from the Mediterranean Sea, Egypt. Egypt J Aquat Res. 2019 Sep;45(3):197–204.
[86] Cruz-Luna AR, Cruz-Martínez H, Vásquez-López A, Medina DI. Metal nanoparticles as novel antifungal agents for sustainable agriculture: Current advances and future directions. J Fungi. 2021 Dec;7(12):1033.

[87] Iqbal J, Abbasi BA, Ahmad R, Shahbaz A, Zahra SA, Kanwal S, et al. Biogenic synthesis of green and cost effective iron nanoparticles and evaluation of their potential biomedical properties. J Mol Struct. 2020 Jan 5;1199:126979.
[88] Ogunsona EO, Muthuraj R, Ojogbo E, Valerio O, Mekonnen TH. Engineered nanomaterials for antimicrobial applications: A review. Appl Mater Today. 2020 Mar;18:100473.
[89] Ahmadi S, Fazilati M, Nazem H, Mousavi SM. Green synthesis of magnetic nanoparticles using Satureja hortensis essential oil toward superior antibacterial/fungal and anticancer performance. BioMed Res Int. 2021 Jan;2021:e8822645.
[90] Rana A, Pathak S, Lim DK, Kim SK, Srivastava R, Sharma SN, et al. Recent advancements in plant- and microbe-mediated synthesis of metal and metal oxide nanomaterials and their emerging antimicrobial applications. ACS Appl Nano Mater. 2023 May;6(10):8106–34.
[91] Arias LS, Pessan JP, Vieira APM, Lima TMTde, Delbem ACB, Monteiro DR. Iron oxide nanoparticles for biomedical applications: A perspective on synthesis, drugs, antimicrobial activity, and toxicity. Antibiotics. 2018 Jun;7(2):46.
[92] Saied E, Salem SS, Al-Askar AA, Elkady FM, Arishi AA, Hashem AH. Mycosynthesis of hematite (α-Fe2O3) nanoparticles using Aspergillus niger and their antimicrobial and photocatalytic activities. Bioengineering. 2022 Aug;9(8):397.
[93] Abbasi BA, Iqbal J, Mahmood T, Qyyum A, Kanwal S. Biofabrication of iron oxide nanoparticles by leaf extract of Rhamnus virgata: Characterization and evaluation of cytotoxic, antimicrobial and antioxidant potentials. Appl Organomet Chem. 2019;33(7):e4947.
[94] Zakariya NA, Majeed S, Jusof WHW. Investigation of antioxidant and antibacterial activity of iron oxide nanoparticles (IONPS) synthesized from the aqueous extract of Penicillium spp. Sens Int. 2022 Jan;3:100164.